I&EC research
Industrial & Engineering Chemistry Research

Article

Cite This: Ind. Eng. Chem. Res. 2017, 56, 13610-13617

pubs.acs.org/IECR

# Sulfurized Graphene as Efficient Metal-Free Catalysts for Reduction of 4-Nitrophenol to 4-Aminophenol

Zhiyong Wang,[†] Rina Su,[†] Dan Wang,*[,†] Jie Shi,[†] Jie-Xin Wang,[†,‡,§] Yuan Pu,*[,‡] and Jian-Feng Chen[†,‡,§]

[†]State Key Laboratory of Organic-Inorganic Composites, [‡]Research Center of the Ministry of Education for High Gravity Engineering and Technology, and [§]Beijing Advanced Innovation Center for Soft Matter Science and Engineering, Beijing University of Chemical Technology, Beijing 100029, China

Supporting Information

**ABSTRACT:** The development of metal-free catalysts for hydrogenation reduction of 4-nitrophenol (4-NP) to 4-aminophenol (4-AP) has been of great increasing scientific and industrial importance. Herein, we reported the preparation of sulfurized graphene (SG) nanomaterials by a well-developed ball-milling method. The as-prepared SG nanomaterials were systematically characterized by scanning electron microscope, transmission electron microscope, Fourier transform infrared, and X-ray photoelectron spectroscopy. The SG exhibited flake-like morphology with average size of 100 nm, and the S doping (3.4 atom %) into the nanocarbon molecules results in asymmetry of electron density distribution, providing high catalytic performance for catalytic reduction of 4-NP to 4-AP by using $NaBH_4$ as the reducer. The related catalytic mechanism and reaction path of the reduction were investigated. The effects of different initial 4-NP concentrations, initial reductant concentrations, catalyst dosages, and reaction temperatures were presented, which have not been reported so far. The thermodynamic parameters including activation enthalpy and entropy were determined.

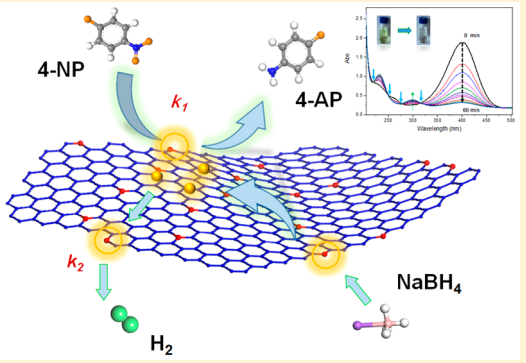


## 1. INTRODUCTION

The compound 4-aminophenol (4-AP), which is conventionally obtained by the reduction of 4-nitrophenol (4-NP), has been known as one of the most important intermediates in pharmaceuticals and dyeing industry.[1] The conventional method for the synthesis of 4-AP involves iron-acid reduction of 4-NP, resulting in serious pollution problems.[2] In recent years, a number of noble metal catalysts have been proved as efficient catalysts for the reduction of 4-NP to 4-AP, such as silver hydrogel,[3] palladium nanoparticles,[4] and gold nanorods.[5] Some nonprecious metal nanocatalysts have also emerged, showing considerable catalytic performance for this reaction.[6,7] However, the scalable industrial applications of metal catalysts are limited, due to the high cost of the catalysts and the metal contamination of the product. The economy of production process is particularly critical in low-value sectors, such as pesticide and dyeing industry.[8] Therefore, developments of efficient metal-free catalysts instead of metal catalysts for the reduction of 4-NP to 4-AP have attracted much attention from both scientific and industrial fields.[9−11]

Carbon based metal-free catalysts, such as fullerenes, carbon nanotubes, and graphene nanosheets, have been demonstrated to be promising alternatives to metal catalysts in various fields.[12−14] Heteroatom doping and loading have been effective ways to tailor the properties of carbon nanomaterials and greatly broadened their application areas.[15−20] For instance, Kong et al. have demonstrated the metal-free catalytic reduction of 4-NP to 4-AP by $NaBH_4$ using nitrogen doped graphene as catalysts.[1] Theoretical calculations verified that the carbon atoms next to the doped N atoms on graphene served as the active sites. In addition to N-doping, sulfur can also tailor the electronic property and chemical reactivity of carbon materials, as well as give rise to new functions. As a matter of fact, S-doped graphene have found applications in oxygen reduction reaction,[21,22] catalytic oxidation reaction,[23] esterification reaction,[24] and photocatalysis,[25] exhibiting pronounced catalytic activity. However, as far as we are aware, studies on using S-doped graphene for the catalytic reduction of 4-NP to 4-AP were rarely reported.

In this work, we reported the preparation of sulfurized graphene (SG) and their catalytic performance as metal-free catalysts for 4-nitrophenol reduction reaction system. The powders of SG nanoplatelets were obtained by a well-developed ball-milling method.[26,27] The morphology and chemical structure of the SG were characterized by various techniques. The SG catalysts were applied to the chemical hydrogenation reduction of 4-NP to 4-AP, which has not been reported so far. The related catalytic mechanism of SG was evaluated by density functional theory (DFT), and the

**Received:** August 3, 2017
**Revised:** September 26, 2017
**Accepted:** October 26, 2017
**Published:** October 26, 2017





DOI: 10.1021/acs.iecr.7b03217
Ind. Eng. Chem. Res. 2017, 56, 13610−13617

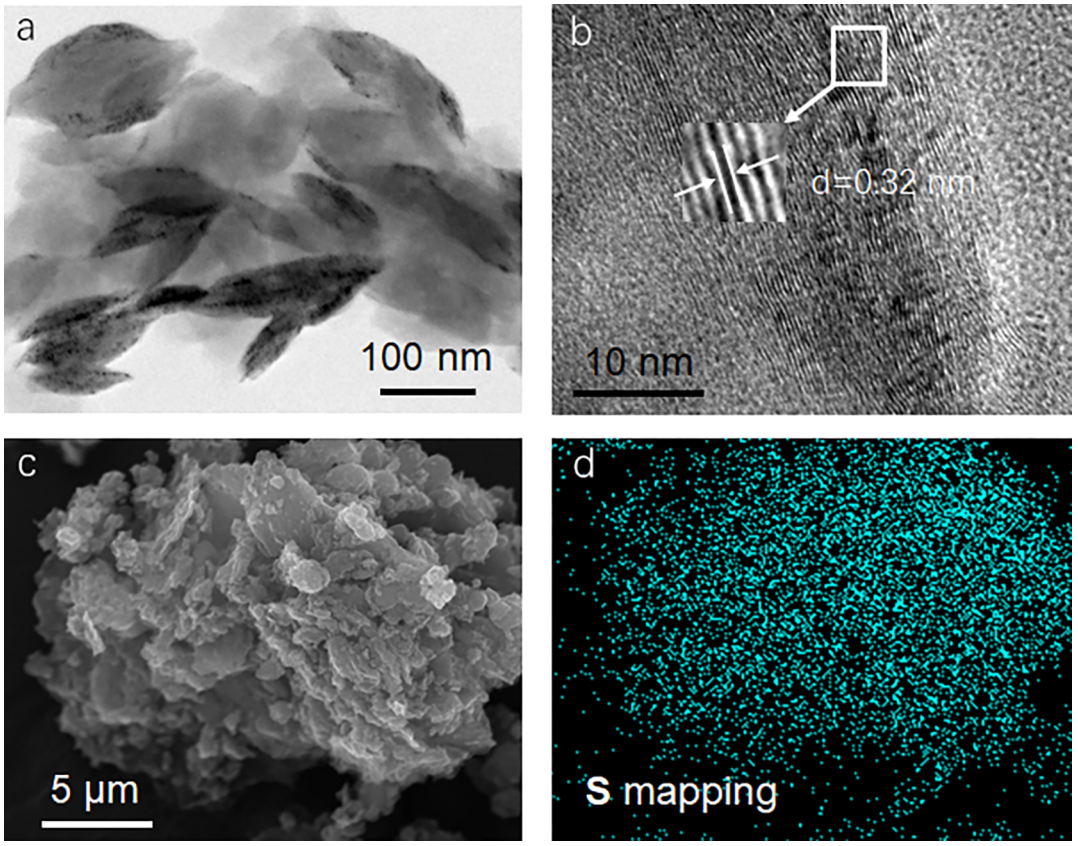


**Figure 1.** (a) TEM image, (b) HRTEM image, (c) SEM image, and (d) sulfur mapping of SG.

performance of using SG as catalysts for the reduction of 4-NP to 4-AP was experimentally investigated. The kinetic factors such as initial 4-NP concentration, initial reductant (sodium borohydride) concentration, and catalyst dosage that affect the catalytic activity were studied. We also determined the thermodynamic parameters including activation enthalpy and entropy by conducting the reaction under different temperatures.

## 2. EXPERIMENTAL SECTION

**2.1. Materials and Instruments.** The pristine graphite flakes (~200 $\mu$m) and sulfur were purchased from Alfa Aesar. Concentrated sulfuric acid, hydrogen nitrate, carbon disulfide, sodium borohydride ($NaBH_4$), and 4-nitrophenol were purchased from Sigma-Aldrich Co. All the reagents were used without further purification, and deionized (DI) water was used in all the experimental procedures. Transmission electron microscope (TEM) images were taken by a Hitachi H-9500 high resolution TEM operating at 300 kV in bright-field mode. The scanning electron microscope (SEM) images and energy-dispersive X-ray (EDX) mapping results were obtained by a Hitachi S-4700 field emission SEM. Fourier transform infrared (FTIR) spectra were measured on a Thermo Fisher Nicolet 6700 FTIR system using samples prepared as KBr pellets. X-ray photoelectron spectroscopy (XPS) measurements were performed on a VG Microtech ESCA 2000.

**2.2. Preparation of SG.** SG nanoparticles were synthesized from commercial graphite with a modified ball-milling method.[26] Briefly, graphite flakes were immersed into the mixed acid of nitric acid and sulfuric acid (1:1 in volume) for 5 h. The obtained chemical modified graphite flakes were then treated at 700 °C to increase the distance of the adjacent graphite layers. The resultant products were mixed with sulfur powder in a planetary mill, which was composed of a stainless steel drum and a number of stainless steel balls with diameter of 5 mm. The ball-milling treatment was then performed by setting agitation of capsule at 500 rpm for overnight. After washing by carbon disulfide to remove the excess sulfur, the products of SG were collected and stored for further use.

**2.3. Catalytic Analysis of SG.** To investigate the catalytic performance of SG for hydrogenation of 4-NP, 1 mg of SG catalysts was added into 40 mL of aqueous solution containing 2 mmol of $NaBH_4$ and 0.02 mmol of 4-NP. To investigate the process of the reaction, 3.5 mL of the mixture was removed to a quartz cuvette (4.5 cm × 1.25 cm × 1.25 cm) at different times (0−60 min, at 5 min intervals). A Shimadzu UV2600 UV−vis spectrometer was used to measure the absorbance spectra of the respective solutions. On the basis of Beer−Lambert law,[28] the absorbance of the peaks at 400 and 300 nm was measured to calibrate the concentrations of 4-NP and 4-AP, respectively.

**2.4. DFT Simulation.** The density functional theory (DFT) calculations were carried out using the Dmol$^3$ code through Materials Studio 8.0 commercial software. The SG model was created based on a graphene sheet including 100 carbon atoms and 25 hydrogen atoms, with one sulfur atom doped at the edge. The adsorption energy ($E_{ads}$) for each reactant was calculated to analyze the relative adsorbability of different materials, according to eq 1.

$$E_{ads} = E_{total} - E_{catalysts} - E_{molecule} \quad (1)$$



DOI: 10.1021/acs.iecr.7b03217
Ind. Eng. Chem. Res. 2017, 56, 13610−13617

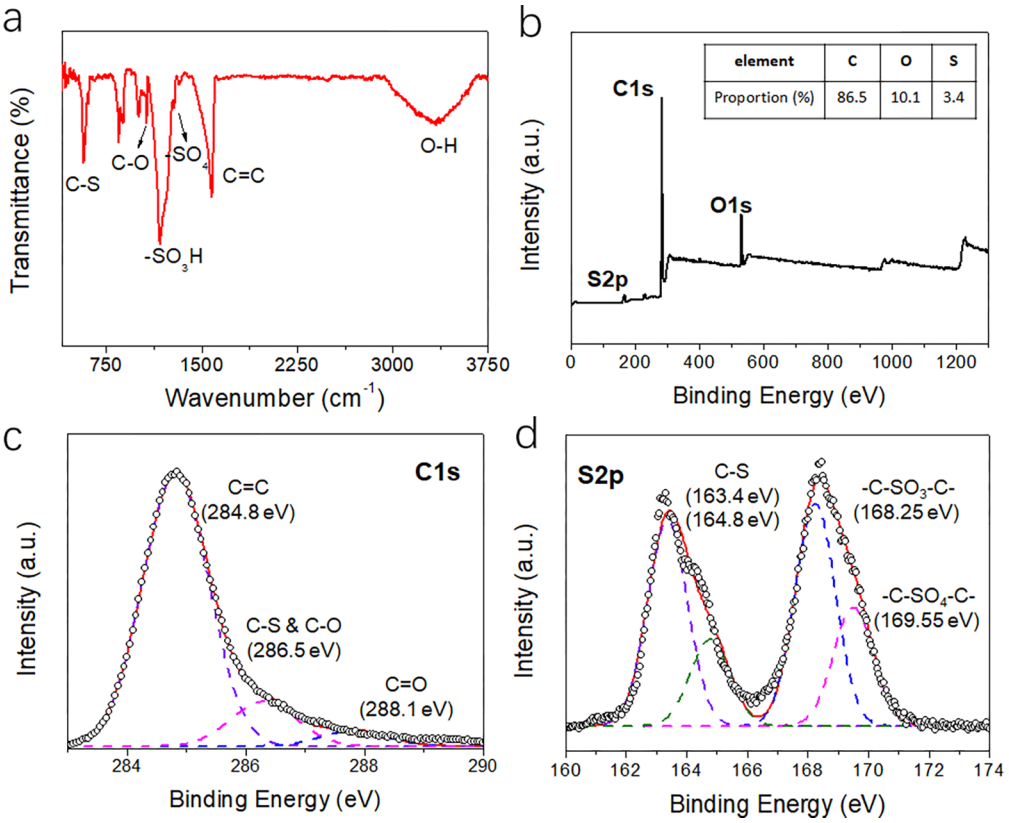


**Figure 2.** (a) Typical FTIR spectrum of SG, (b) XPS spectrum of SG (inset, the percentage ratio of C, O, S atoms), (c) high resolution C 1s peak, and (d) high resolution S 2p peak.

where $E_{total}$ is the total energy of the optimized system, $E_{catalysts}$ is the energy of the catalysts, and $E_{molecule}$ is the energy of the adsorbed molecule.

## 3. RESULTS AND DISCUSSION

Figure 1a presents a typical TEM image of the SG, which exhibited flake-like morphology with average size of 100 nm. The high resolution TEM image (Figure 1b) shows a lattice fringe spacing of 0.32 nm, which was in agreement with the diffraction planes of $sp^2$ graphitic carbon.[15] The SEM image and EDX mapping results demonstrated the uniform distribution of sulfur element on the graphene nanoplates. These results are consistent with those of SG previously reported in the literature.[26,27]

The FTIR bands centered at approximately 581 $cm^{-1}$ for the SG sample were attributed to the stretching vibrations of the C−S bond,[23] indicating the doping of sulfur in the graphene sheets (Figure 2a). Two peaks at approximately 1070 and 1576 $cm^{-1}$ were assigned to the stretching C−O and C═C bonds, respectively. The bands at around 3342, 1178, and 1277 $cm^{-1}$ showed the presence of oxygen-containing functional groups (−OH, $-SO_3H$, and $-SO_4$) to render the SG soluble in water. Furthermore, the XPS spectrum of the SG in Figure 2b shows a pronounced C 1s peak at 284 eV and O 1s peak at 533 eV, with small amounts of S (3.4 atom %) arising due to the S-doping. A high resolution C 1s peak in Figure 2c was fitted to three component peaks located at about 284.8, 286.5, and 288.1 eV, corresponding to the graphite C−C, C−S and C−O, and C═O bond, respectively.[27] Figure 2d presented the high resolution peak separation of S 2p, demonstrating the C−S, $-C-SO_3-C-$, and $-C-SO_4-C-$ at 163.4, 168.25, and 169.55 eV, respectively. In addition, two types of C−S fitting peak at 228 and 233 eV for S 2s spectrum, which correspond to the C−S fitting peaks at 163.4 and 164.8 eV for S 2p spectrum, respectively, indicated the natural bonding between sulfur and graphite at the edges of SG nanoplates (Figure S1).[29,30]

The hydrogenation reduction of 4-NP to 4-AP in the presence of excess $NaBH_4$, which is an important organic catalytic reaction, was carried out to evaluate the catalytic performance of SG metal-free catalyst. To start with, 3 mg of 4-NP powder was dissolved in 40 mL of deionized water; after sonication for half an hour, the solution was light yellow and the UV−vis spectrum shows an absorption peak centered at 318 nm. With the addition of $NaBH_4$ (120 mg) into the 4-NP solution, the color of the mixture changed from light yellow to dark yellow and the maximum absorption peak shifted from 310 to 400 nm, which was attributed to the formation of 4-nitrophenolate (Figure 3a).[31] In the absence of SG catalysts, a small amount of bubbles were observed because of the hydrogen generation by the reduction reaction between $NaBH_4$ and water (Figure S2a). However, in the presence of SG catalysts, a large amount of bubbles were observed and the gas release rate became much faster (Figure S2b). Ultimately, after reacting for 60 min and filtering the SG from the mixture by microfilter (diameter of 0.45 $\mu$m), the solution became colorless and transparent. It illustrates that the 4-NP was completely converted to 4-AP. The whole reaction process was monitored by UV−vis spectra, and the results were shown in Figure 3b. The absorption intensity of 4-NP peak at 400 nm decreased, and the absorption peak of 4-AP located at 300 nm appeared. Four isoabsorptive points at 223, 245, 278, and 314 nm were observed, illustrating no byproduct generation.[1] The



DOI: 10.1021/acs.iecr.7b03217
Ind. Eng. Chem. Res. 2017, 56, 13610−13617

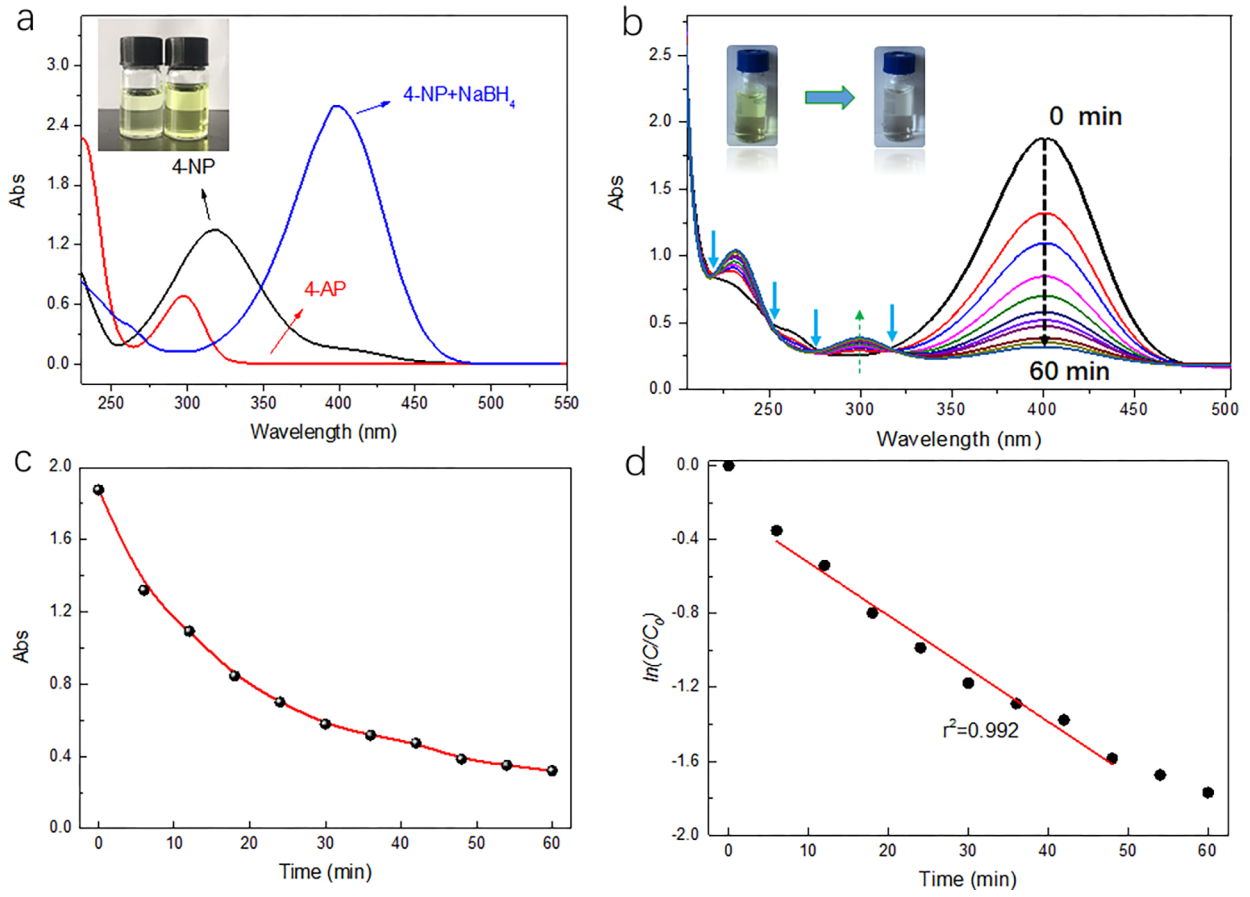


**Figure 3.** (a) Typical UV/vis spectra of aqueous solutions of 4-NP, 4-NP with $NaBH_4$, and 4-AP, with inset showing a digital photo of the solution of 4-NP (left) and 4-NP with $NaBH_4$ (right), (b) UV/vis spectra changes of aqueous solution of 4-NP in the presence of $NaBH_4$ and SG for various times, (c) the curves of absorption intensity (at 400 nm) as a function of time, and (d) the curves of $\ln(C/C_0)$ as a function of time. (Reaction conditions: $c_{4\text{-NP}}$:$c_{NaBH_4}$ = 1:100, room temperature, $m_{SG}$ = 1 mg, volume of reaction mixture was 40 mL).

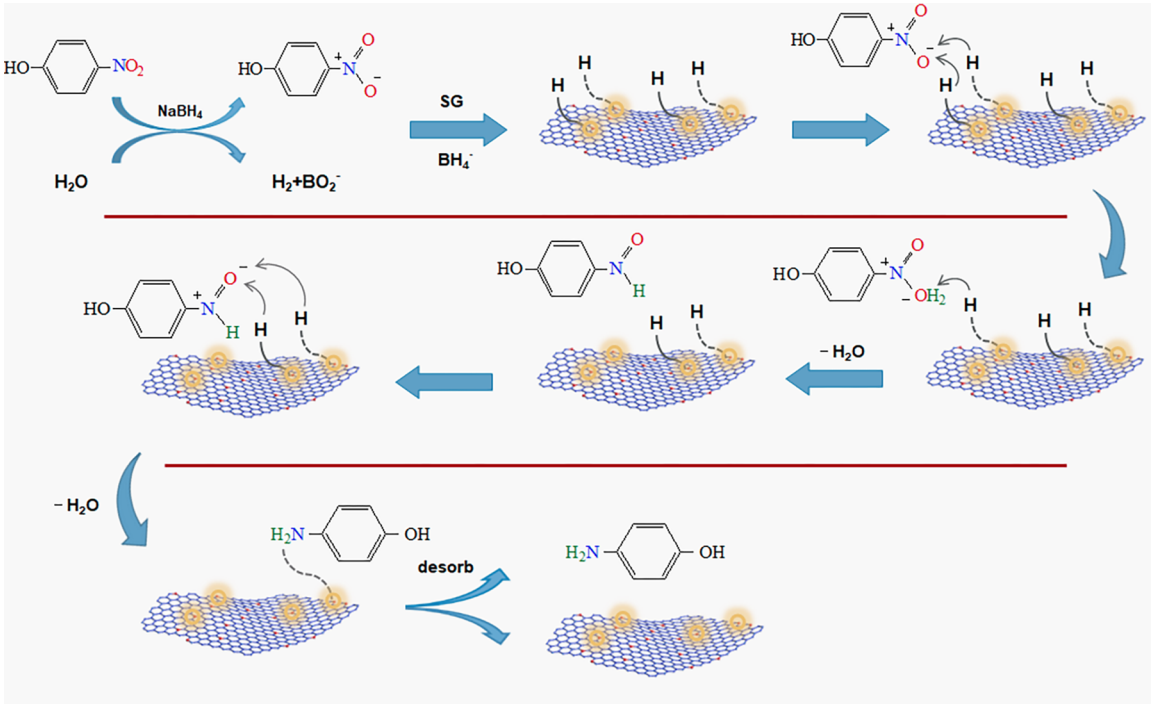


**Figure 4.** Proposed route for the metal-free catalytic reduction of 4-NP to 4-AP by using $NaBH_4$ as the reducer.



DOI: 10.1021/acs.iecr.7b03217
Ind. Eng. Chem. Res. 2017, 56, 13610−13617

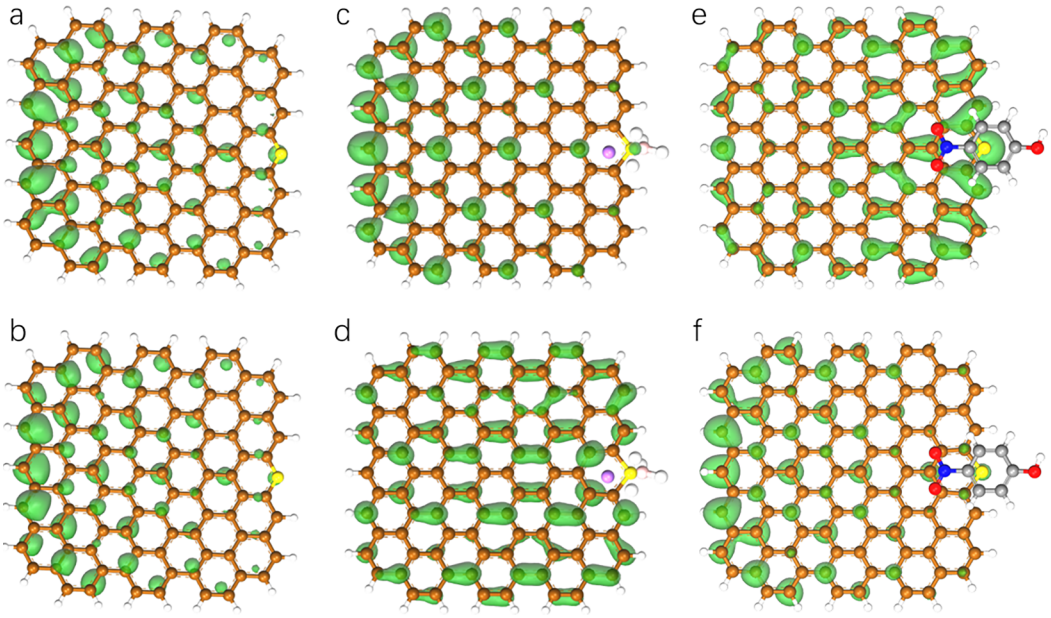


**Figure 5.** (a) HOMO and (b) LUMO of SG; (c) HOMO and (d) LUMO of $NaBH_4$ adsorbed on SG; (e) HOMO and (f) LUMO of 4-NP adsorbed on SG. The brown, blue, yellow, red, and white balls stand for C, N, S, O, and H atoms, respectively.

linear fitting degree of $C/C_0$ versus time and $\ln(C/C_0)$ versus time were presented in Figure 3c and Figure 3d, respectively. As can be seen, the catalytic reaction of 4-NP to 4-AP by $NaBH_4$ in the presence of SG catalysts obeyed pseudo-first-order kinetics. The value of the apparent kinetic rate constant ($k_{app}$) was then calculated by eq 2.

$$\ln\left(\frac{A}{A_0}\right) = \ln\left(\frac{C}{C_0}\right) = k_{app}t \tag{2}$$

where $A$ and $A_0$ are the absorbance of 4-NP at 400 nm at any time and at 0 min, respectively. $C$ and $C_0$ are the concentration of 4-NP in the solution corresponding to $A$ and $A_0$, respectively.

The apparent rate constant of the reaction in our experiment was calculated to be 0.028 74 $min^{-1}$ from the slope fitted by plotting of $\ln(C/C_0)$ versus time (Figure 3d). Moreover, the specific rate constant was $5.95 \times 10^{-5}$ mol $L^{-1}$ $s^{-1}$ $g^{-1}$, which is comparable to that of nitrogen-doped graphene ($8.09 \times 10^{-5}$ mol $L^{-1}$ $s^{-1}$ $g^{-1}$).[32] The reusability and stability of SG were also investigated (Supporting Information). A 40% decrease in $k_{app}$ was observed after using the SG for six cycles (Figure S4a and Figure S4b), which was attributed to the effect of reaction products that were hard to be separated from the SG (Figure S3).

The reaction mechanism of 4-NP catalytic reduction by $NaBH_4$ in the presence of metal catalysts has been proposed in previous literature.[3,6,7] However, the reaction routes of 4-NP reduction by metal-free catalysts, in particular sulfur-doped carbon materials, have been rarely reported. Herein, we proposed an experimental route for the 4-NP reduction by $NaBH_4$ using SG as metal-free catalysts. As the schematic shown in Figure 4, the $NaBH_4$ first hydrolyzes in water to form borohydride ions, which then give electrons to the SG catalysts, generating active hydrogen species on the surface of SG. Followed by the adsorption of 4-NP on SG, the 4-NP is reduced by the active hydrogen species. In general, 4-hydroxylaminophenol, which in the form of transition state, was then converted into 4-aminophenol. Finally, the 4-aminophenol was desorption from the catalyst surface, which can provide free site for the next catalytic cycle.

To further understand the fundamental role of SG for the catalytic process of 4-NP reduction, a chemical structure optimization of SG was performed by density functional theory (DFT) methods. The model of SG was based on a graphene sheet including 100 carbon atoms and 25 hydrogen atoms. As previously reported, the catalytic activity of the heteroatom doped graphene is closely related to the orbital distributions on the graphitic framework.[30] Therefore, the highest occupied molecular orbital (HOMO) and the lowest unoccupied molecular orbital (LUMO) distributions, which represent capability of electron donating and accepting, respectively, were calculated on the SG models. For the pristine graphene, the HOMO and LUMO orbitals are all uniformly distributed on the framework (Figure S5). However, in stark contrast, the HOMO and LUMO orbitals are polarized when the sulfur atom was doped on the graphene plane (Figure 5a and Figure 5b), which was attributed to the strong covalent action between C atoms and S atom at the edge of graphene sheet. The polarization region may serve as the active sites for the catalytic reduction of 4-NP. The HOMO and LUMO distributions on the SG after $NaBH_4$ adsorbed were shown in Figure 5c and Figure 5d, respectively. It was obviously noted that the LUMO distribution around the S atom was increased while the HOMO showed no significant change, illustrating that the $NaBH_4$ acts as an electron donor during the reduction process. On the other hand, Figure 5e and Figure 5f show sharp increasing of HOMO around S atom with invariant distributions of LUMO when the 4-NP molecule was adsorbed on SG, indicating that 4-NP gains electrons in the reaction.[33] Furthermore, Table S1 shows that the adsorption energy ($E_{ads}$) of $NaBH_4$ was −0.59 eV, which is slight larger than that of 4-NP (−0.57 eV). However, the molecular weight of 4-NP is greater than that of sodium borohydride; thus $NaBH_4$ is easier adsorbed on SG nanoplates. These results are in good agreement with the above assumed reaction mechanism.



DOI: 10.1021/acs.iecr.7b03217
Ind. Eng. Chem. Res. 2017, 56, 13610−13617

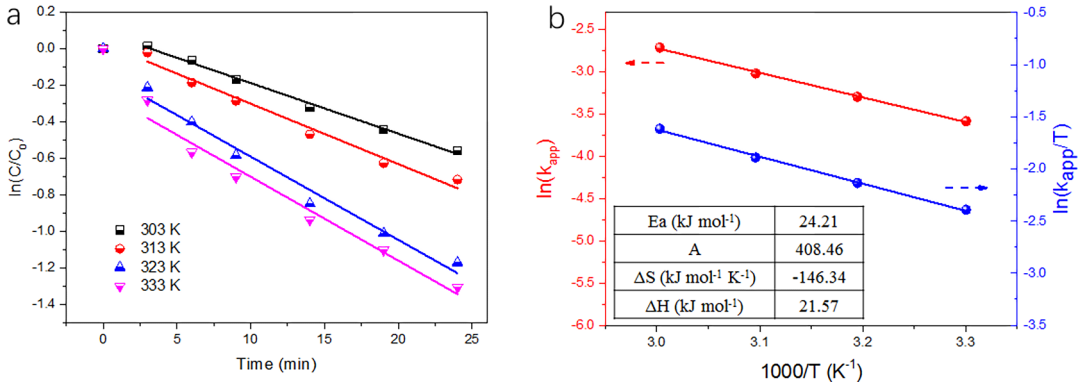


**Figure 6.** (a) $\ln(C/C_0)$ versus time at different reaction temperature. (b) $\ln(k_{app})$ (red line) and $\ln(k_{app}/T)$ (blue line) versus $1/T$, with inset showing the values of thermodynamic parameters.

The catalytic thermodynamic parameters for the reduction of 4-NP by SG was then studied by conducting the reaction at various temperatures (30, 40, 50, and 60 °C) with 3.5 mL of reactant; it is apparently seen in Figure 6a that there is a higher $k_{app}$ for the reaction at a higher temperature, which can be explained by collision theory. The 4-NP molecules moved around by free diffusion with a certain chance to collide with each other. The colliding molecule may react when the energy of the reaction mixture is in excess to the reaction activation energy. When temperature of the system increases, the movement of molecules will be more violent, leading to a greater chance for collision, which results in the faster reaction rate.[34] The apparent activation energy ($E_a$) and thermodynamic parameters were calculated using the Arrhenius and Eyring equations as the following.

$$\ln k_{app} = \ln A - \frac{E_a}{RT} \tag{3}$$

$$\ln\left(\frac{k_{app}}{T}\right) = \frac{\Delta S}{R} - \frac{\Delta H}{R}\left(\frac{1}{T}\right) + \ln\left(\frac{k_B}{\hbar}\right) \tag{4}$$

where $E_a$ is apparent activation energy, $A$ is the pre-exponential factor, $R$ is the general gas constant ($R$ = 8.314 J·K$^{-1}$·mol$^{-1}$), $k_B$ (the value of 1.38 × 10$^{-23}$ J K$^{-1}$) and $\hbar$ (the value of 6.63 × 10$^{-34}$ J) are the Boltzmann and Planck constants, respectively, and $\Delta S$ and $\Delta H$ are the activation entropy and enthalpy, respectively.

The values of $E_a$, which can illustrate the influence of temperature on apparent reaction rate, is an important parameter in a catalytic reaction. As shown in Table 1, the $E_a$ for SG catalyzed reaction was calculated as 24.21 kJ mol$^{-1}$, indicating that the reduction of 4-NP in the SG catalytic system occurs via surface reaction.[7] In general, a lower activation energy ($E_a$) leads to a higher reaction rate. However, there was no absolute correlation between $E_a$ and reaction rate.[35] For example, $CeO_2$/CuNi displays the highest catalytic performance although it possesses the highest $E_a$. Therefore, it would be not comprehensive to evaluate the catalytic performance of the catalyst only by determining activation energy. But one thing is certain, the SG is an efficient metal-free catalyst that can be compared with most of the conventional catalysts. The values of $\Delta S$ and $\Delta H$ can obtained to be −146.34 kJ mol$^{-1}$ K$^{-1}$ and 21.57 kJ mol$^{-1}$ according to the plot of $\ln(k_{app})$ and $\ln(k_{app}/T)$ versus $1/T$, respectively (inset of Figure 6b). The number of surface active sites of SG is an important influence factor for $k_{app}$, since the catalytic reduction of 4-NP is a surface transfer reaction as mentioned above. The detection of the number of surface active sites would be helpful for the development of high performance metal-free SG catalysts, which should be good topics for future studies in materials science and engineering.

**Table 1. Comparative Study of the Activation Energy and Catalytic Activity of SG for Reduction of 4-Nitrophenol**[a]

| entry | catalyst | $E_a$ (kJ mol$^{-1}$) | $k_{app}$ (min$^{-1}$) | ref |
|---|---|---|---|---|
| 1 | $CeO_2$/CuNi | 39.695 | 9.928 | 7 |
| 2 | acrylic acid-amidodiol/Ag hydrogel (SPAG) | 28 | 0.489 | 3 |
| 3 | porous Cu microspheres | 31.9 | 0.316 | 36 |
| 4 | silver nanoparticles | 33.8 | 0.160 | 37 |
| 5 | N doped graphene foam (metal free) | 33.8 | 0.239 | 10 |
| 6 | SG (metal free) | 24.21 | 0.317 | this work |

[a]The $k_{app}$ in different references were converted according to the actual reaction conditions. Here, the standard reaction conditions are the following: $c_{4\text{-NP}}$:$c_{NaBH_4}$ = 1:100, $T$ = 25 °C, $m_{SG}$ = 3 mg, the volume of reaction mixture was 3.5 mL.

It has been reported that the initial concentrations of 4-NP, sodium hydroxide, and catalyst dosage occupy an important position for the catalytic reduction of 4-NP to 4-AP by typical metal based catalysts.[7,38] However, to the best of our knowledge, there is currently no report about the kinetics research for this catalytic reaction system catalyzed by a SG metal-free catalyst. To investigate the effect of reaction conditions on $k_{app}$, the experiments were carried out by varying the catalyst dosage, initial 4-NP concentration, and sodium hydroxide concentration at room temperature with a single factor method. As the described above, the catalytic reduction of 4-NP is a surface transfer reaction, and the number of surface active sites of SG is an important influence factor for $k_{app}$. Moreover, as the same condition for the preparation of SG and its well dispersion, the quantity of active sites is proportional to catalyst dosage. Thus it is expected, as shown in Figure 7a, that the value of $k_{app}$ is positively related to the augment of catalyst dosage.

Figure 7b displays the dependence of $\ln(C/C_0)$ on time at different initial 4-NP concentrations. Apparently, the value of $k_{app}$ is monotonically decreased with the increasing of initial 4-NP concentration. The coadsorption for the reactant and reductant on the surface active sites is one of the requirements


DOI: 10.1021/acs.iecr.7b03217
Ind. Eng. Chem. Res. 2017, 56, 13610−13617

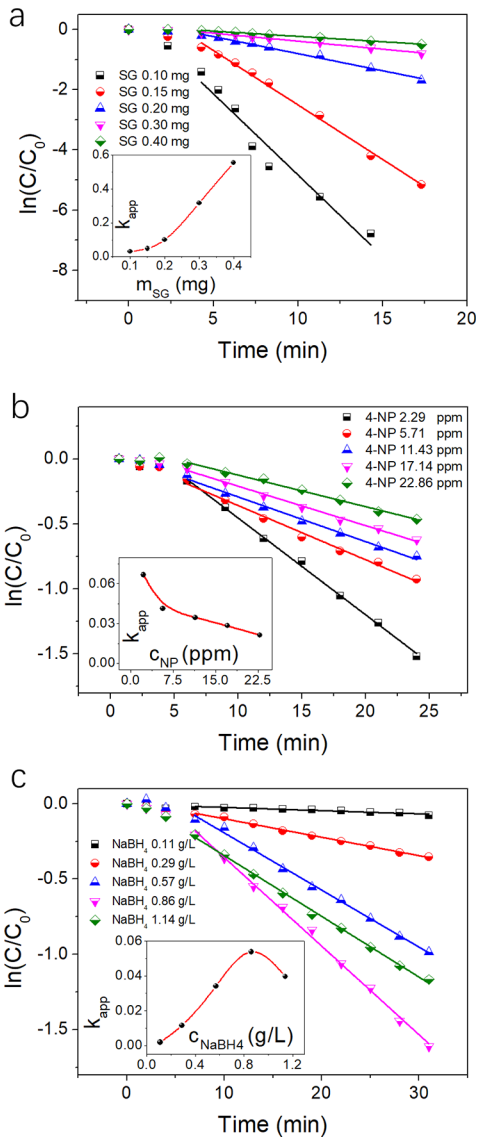


**Figure 7.** Plots of $\ln(C/C_0)$ versus time with (a) dosage of SG and different concentration of (b) 4-NP and (c) $NaBH_4$. The inset images of parts a–c display the values of $k_{app}$ versus catalyst dosage, 4-NP concentration, and $NaBH_4$ concentration, respectively.

for the occurrence of the reaction. When the 4-NP concentration in the solution is low, there is a small number of 4-NP molecules that can be adsorbed on the SG sheet surface because most of active sites were occupied by $NaBH_4$; therefore, the conversion for the adsorbed 4-NP is easy. However, as the concentration of 4-NP increased, more and more 4-NP molecules occupy the active sites, resulting in fewer formation of surface active hydrogen species and a low reaction rate. As exhibited in Figure 7c, the $k_{app}$ increases with concentration of $NaBH_4$ up to around 0.8 g $L^{-1}$ and then decreases as the concentration is increased sequentially. According to the mechanism expressed in Figure 4, when the initial concentration of 4-NP is unchanged, the chance for the reaction to occur increased with the concentration of $NaBH_4$ up to a certain value (0.8 g $L^{-1}$), which is due to the synchronous increase of reductant and surface active hydrogen species. However, as the concentration of $NaBH_4$ is further increased, the rest of the $NaBH_4$ molecules and 4-NP molecules begin to compete with each other to adsorb on the SG sheet, resulting in a little reduced value of $k_{app}$.

## 4. CONCLUSIONS

In summary, sulfurized graphene (SG) nanomaterials were prepared by a well-developed ball-milling method and systematically characterized by scanning electron microscope, transmission electron microscope, Fourier transform infrared, and X-ray photoelectron spectroscopy. The SG exhibited flake-like morphology with average size of 100 nm. The S content in the SG was 3.4 atom % with uniform distribution, providing high catalytic performance for catalytic reduction of 4-NP to 4-AP by using $NaBH_4$ as the reducer. The kinetics studies of the reaction process were investigated by single factor method at various conditions including catalyst dosages, initial 4-NP concentration, and initial reductant concentration. Furthermore, the catalytic thermodynamic parameters for the reduction of 4-NP by SG was studied by conducting the reaction at various temperatures, and the apparent activation energy ($E_a$) of this reaction system was calculated as 24.21 kJ $mol^{-1}$. The thermodynamics parameters including $\Delta S$ and $\Delta H$ were also obtained from the Eyring equation. Our results show that as-synthesized SG nanomaterials are promising metal-free catalysts for hydrogenation reduction of 4-NP to 4-AP.

## ■ ASSOCIATED CONTENT

### Supporting Information

The Supporting Information is available free of charge on the ACS Publications website at DOI: 10.1021/acs.iecr.7b03217.

Figures showing high resolution XPS peak fit for S 2s peak of SG, photograph of a reaction solution with or without SG, hydrogen generation rate with and without SG, photograph of reaction mixture after centrifugal treatment for 10 min at 10 000 rpm, curves of $\ln(C/C_0)$ as a function of time for different cycles, catalyst stability at different cycles, and HOMO and LUMO of pristine graphene; table showing the simulated adsorption energy of 4-NP and $NaBH_4$ on SG model (PDF)

## ■ AUTHOR INFORMATION


### Corresponding Authors

*D.W.: tel, +86-10-64449453; e-mail, wangdan@mail.buct.edu.cn.

*Y.P.: tel, +86-10-64421905; e-mail, puyuan@mail.buct.edu.cn.

### ORCID

Dan Wang: 0000-0002-3515-4590

Jie-Xin Wang: 0000-0003-0459-1621


### Notes

The authors declare no competing financial interest.

## ■ ACKNOWLEDGMENTS

We are grateful for financial support from National Natural Science Foundation of China (Grants 21620102007 and 21622601), the Fundamental Research Funds for the Central Universities of China (Grant BUCTRC201601), and the "111" Project of China (Grant B14004).

## ■ REFERENCES

(1) Kong, X.; Sun, Z.; Chen, M.; Chen, C.; Chen, Q. Metal-Free Catalytic Reduction of 4-Nitrophenol to 4-Aminophenol by N-Doped Graphene. *Energy Environ. Sci.* **2013**, *6*, 3260.



DOI: 10.1021/acs.iecr.7b03217
*Ind. Eng. Chem. Res.* 2017, 56, 13610–13617

(2) Rode, C. V.; Vaidya, M. J.; Chaudhari, R. V. Synthesis of p-Aminophenol by Catalytic Hydrogenation of Nitrobenzene. *Org. Process Res. Dev.* **1999**, *3*, 465.
(3) Narayanan, R. K.; Devaki, S. J. Brawny Silver-Hydrogel Based Nanocatalyst for Reduction of Nitrophenols: Studies on Kinetics and Mechanism. *Ind. Eng. Chem. Res.* **2015**, *54*, 1197.
(4) Park, H.; Reddy, D. A.; Kim, Y.; Lee, S.; Ma, R.; Lim, M.; Kim, T. K. Hydrogenation of 4-Nitrophenol to 4-Aminophenol at Room Temperature: Boosting Palladium Nanocrystals Efficiency by Coupling with Copper via Liquid Phase Pulsed Laser Ablation. *Appl. Surf. Sci.* **2017**, *401*, 314.
(5) Mohanta, J.; Satapathy, S.; Si, S. Porous Silica-Coated Gold Nanorods: A Highly Active Catalyst for the Reduction of 4-Nitrophenol. *ChemPhysChem* **2016**, *17*, 364.
(6) Xia, F.; Xu, X.; Li, X.; Zhang, L.; Zhang, L.; Qiu, H.; Wang, W.; Liu, Y.; Gao, J. Preparation of Bismuth Nanoparticles in Aqueous Solution and Its Catalytic Performance for the Reduction of 4-Nitrophenol. *Ind. Eng. Chem. Res.* **2014**, *53*, 10576.
(7) Kohantorabi, M.; Gholami, M. R. Kinetic Analysis of the Reduction of 4-Nitrophenol Catalyzed by $CeO_2$ Nanorods-Supported CuNi Nanoparticles. *Ind. Eng. Chem. Res.* **2017**, *56*, 1159.
(8) Yuan, B.; Ren, S.; Chen, X. Can Environmental Regulation Promote the Coordinated Development of Economy and Environment in China's Manufacturing Industry?-A Panel Data Analysis of 28 Sub-Sectors. *J. Cleaner Prod.* **2017**, *149*, 11.
(9) Martin-Martinez, M.; Barreiro, M. F.; Silva, A. T.; Figueiredo, J. L.; Faria, J. L.; Gomes, H. T. Lignin-Based Activated Carbons as Metal-Free Catalysts for the Oxidative Degradation of 4-Nitrophenol in Aqueous Solution. *Appl. Catal., B* **2017**, *219*, 372.
(10) Liu, J.; Yan, X.; Wang, L.; Kong, L.; Jian, P. Three-Dimensional Nitrogen-Doped Graphene Foam as Metal-Free Catalyst for the Hydrogenation Reduction of p-Nitrophenol. *J. Colloid Interface Sci.* **2017**, *497*, 102.
(11) Navalon, S.; Dhakshinamoorthy, A.; Alvaro, M.; Antonietti, M.; García, H. Active Sites on Graphene-Based Materials as Metal-Free Catalysts. *Chem. Soc. Rev.* **2017**, *46*, 4501.
(12) Liu, X.; Dai, L. Carbon-Based Metal-Free Catalysts. *Nat. Rev. Mater.* **2016**, *1*, 16064.
(13) Dai, L.; Xue, Y.; Qu, L.; Choi, H. J.; Baek, J. B. Metal-Free Catalysts for Oxygen Reduction Reaction. *Chem. Rev.* **2015**, *115*, 4823.
(14) Su, D. S.; Zhang, J.; Frank, B.; Thomas, A.; Wang, X.; Paraknowitsch, J.; Schlögl, R. Metal-Free Heterogeneous Catalysis for Sustainable Chemistry. *ChemSusChem* **2010**, *3*, 169.
(15) Wang, D.; Wang, Z.; Zhan, Q.; Pu, Y.; Wang, J.; Foster, N.; Dai, L. Facile and Scalable Preparation of Fluorescent Carbon Dots for Multifunctional Applications. *Engineering* **2017**, *3*, 402.
(16) Wang, D.; Zhu, L.; McCleese, C.; Burda, C.; Chen, J. F.; Dai, L. Fluorescent Carbon Dots from Milk by Microwave Cooking. *RSC Adv.* **2016**, *6*, 41516.
(17) Wang, D.; Liu, J.; Chen, J. F.; Dai, L. Surface Functionalization of Carbon Dots with Polyhedraloligomericsilsesquioxane (POSS) for Multifunctional Applications. *Adv. Mater. Interfaces* **2016**, *3*, 1500439.
(18) Tan, M.; Yang, G.; Wang, T.; Vitidsant, T.; Li, J.; Wei, Q.; Ai, P.; Wu, M.; Zheng, J.; Tsubaki, N. Active and Regioselective Rhodium Catalyst Supported on Reduced Graphene Oxide for 1-Hexene Hydroformylation. *Catal. Sci. Technol.* **2016**, *6*, 1162.
(19) Zhao, Q.; Bai, C.; Zhang, W.; Li, Y.; Zhang, G.; Zhang, F.; Fan, X. Catalytic Epoxidation of Olefins with Graphene Oxide Supported Copper (Salen) Complex. *Ind. Eng. Chem. Res.* **2014**, *53*, 4232.
(20) Zhao, Q.; Chen, D.; Li, Y.; Zhang, G.; Zhang, F.; Fan, X. Rhodium Complex Immobilized on Graphene Oxide as an Efficient and Recyclable Catalyst for Hydrogenation of Cyclohexene. *Nanoscale* **2013**, *5*, 882.
(21) Yang, S.; Zhi, L.; Tang, K.; Feng, X.; Maier, J.; Müllen, K. Efficient Synthesis of Heteroatom (N or S)-Doped Graphene Based on Ultrathin Graphene Oxide-Porous Silica Sheets for Oxygen Reduction Reactions. *Adv. Funct. Mater.* **2012**, *22*, 3634.
(22) Xu, J.; Ma, J.; Fan, Q.; Guo, S.; Dou, S. Recent Progress in the Design of Advanced Cathode Materials and Battery Models for High-PerformaCnce Lithium-X (X = $O_2$, S, Se, Te, $I_2$, $Br_2$) Batteries. *Adv. Mater.* **2017**, *29*, 1606454.
(23) Duan, X.; O'Donnell, K.; Sun, H.; Wang, Y.; Wang, S. Sulfur and Nitrogen Co-Doped Graphene for Metal-Free Catalytic Oxidation Reactions. *Small* **2015**, *11*, 3036.
(24) Wang, Y.; Wang, D.; Tan, M.; Jiang, B.; Zheng, J.; Tsubaki, N.; Wu, M. Monodispersed Hollow $SO_3H$-Functionalized Carbon/Silica as Efficient Solid Acid Catalyst for Esterification of Oleic Acid. *ACS Appl. Mater. Interfaces* **2015**, *7*, 26767.
(25) Qu, D.; Zheng, M.; Du, P.; Zhou, Y.; Zhang, L.; Li, D.; Tan, H.; Zhao, Z.; Xie, Z.; Sun, Z. Highly Luminescent S, N Co-Doped Graphene Quantum Dots with Broad Visible Absorption Bands for Visible Light Photocatalysts. *Nanoscale* **2013**, *5*, 12272.
(26) Lin, T.; Tang, Y.; Wang, Y.; Bi, H.; Liu, Z.; Huang, F.; Xie, X.; Jiang, M. Scotch-Tape-Like Exfoliation of Graphite Assisted with Elemental Sulfur and Graphene-Sulfur Composites for High-Performance Lithium-Sulfur Batteries. *Energy Environ. Sci.* **2013**, *6*, 1283.
(27) Xu, J.; Shui, J.; Wang, J.; Wang, M.; Liu, H. K.; Dou, S. X.; Jeon, I. Y.; Seo, J. M.; Baek, J. B.; Dai, L. Sulfur-Graphene Nanostructured Cathodes via Ball-Milling for High Performance Lithium-Sulfur Batteries. *ACS Nano* **2014**, *8*, 10920.
(28) Pu, Y.; Cai, F.; Wang, D.; Li, Y.; Chen, X.; Maimouna, A. G.; Wu, Z.; Wen, X.; Chen, J. F.; Foster, N. R. Solubility of Bicalutamide, Megestrol Acetate, Prednisolone, Beclomethasone Dipropionate and Clarithromycin in Subcritical Water at Different Temperatures from 383.15 to 443.15 K. *J. Chem. Eng. Data* **2017**, *62*, 1139.
(29) Wang, C.; Su, K.; Wan, W.; Guo, H.; Zhou, H.; Chen, J.; Zhang, X.; Huang, Y. High Sulfur Loading Composite Wrapped by 3D Nitrogen-Doped Graphene as a Cathode Material for Lithium-Sulfur Batteries. *J. Mater. Chem. A* **2014**, *2*, 5018.
(30) Jeon, I. Y.; Zhang, S.; Zhang, L.; Choi, H. J.; Seo, J. M.; Xia, Z.; Dai, L.; Baek, J. B. Edge-Selectively Sulfurized Graphene Nanoplatelets as Efficient Metal-Free Electrocatalysts for Oxygen Reduction Reaction: The Electron Spin Effect. *Adv. Mater.* **2013**, *25*, 6138.
(31) Wu, G.; Liang, X.; Zhang, L.; Tang, Z.; Almamun, M.; Zhao, H.; Su, X. Fabrication of Highly Stable Metal Oxide Hollow Nanospheres and Their Catalytic Activity Toward 4-Nitrophenol Reduction. *ACS Appl. Mater. Interfaces* **2017**, *9*, 18207.
(32) Vinoth, R.; Babu, S. G.; Bahnemann, D.; Neppolian, B. Nitrogen Doped Reduced Graphene Oxide Hybrid Metal Free Catalyst for Effective Reduction of 4-Nitrophenol. *Sci. Adv. Mater.* **2015**, *7*, 1443.
(33) Li, B.; Su, D. Theoretical Studies on Ethylene Selectivity in the Oxidative Dehydrogenation Reaction on Undoped and Doped Nanostructured Carbon Catalysts. *Chem. - Asian J.* **2013**, *8*, 2605.
(34) Nemanashi, M.; Meijboom, R. Synthesis and Characterization of Cu, Ag and Au Dendrimer-Encapsulated Nanoparticles and their Application in the Reduction of 4-Nitrophenol to 4-Aminophenol. *J. Colloid Interface Sci.* **2013**, *389*, 260.
(35) Noh, J. H.; Meijboom, R. Catalytic Evaluation of Dendrimer-Templated Pd Nanoparticles in the Reduction of 4-Nitrophenol Using Langmuir-Hinshelwood Kinetics. *Appl. Surf. Sci.* **2014**, *320*, 400.
(36) Gao, S. Y.; Jia, X. X.; Yang, J. M.; Wei, X. J. Hierarchically Micro/Nanostructured Porous Metallic Copper: Convenient Growth and Superhydrophilic and Catalytic Performance. *J. Mater. Chem.* **2012**, *22*, 21733.
(37) Butun, S.; Sahiner, N. A Versatile Hydrogel Template for Metal Nanoparticle Preparation and their Use in Catalysis. *Polymer* **2011**, *52*, 4834.
(38) Chen, L.; Hu, J.; Qi, Z.; Fang, Y.; Richards, R. Gold Nanoparticles Intercalated into the Walls of Mesoporous Silica as a Versatile Redox Catalyst. *Ind. Eng. Chem. Res.* **2011**, *50*, 13642.


DOI: 10.1021/acs.iecr.7b03217
*Ind. Eng. Chem. Res.* 2017, 56, 13610−13617